

# Amplified warming of extreme temperatures over tropical land

Michael Byrne<sup>1</sup>

<sup>1</sup>University of St Andrews

November 21, 2022

## Abstract

Extreme temperatures have warmed substantially over recent decades and are projected to continue warming in response to future climate change. Warming of extreme temperatures is amplified over land where the impacts on human health, wildfire risk and food production are most severe. Using simulations with climate models, I show that hot days over tropical land warm substantially more than the average day. For example, warming of the hottest 1% of land days is 24% larger than the time-mean warming averaged across models. The climate-change response of extreme temperatures over tropical land is interpreted using a theory based on atmospheric dynamics. According to the theory, warming is amplified for hot land days because those days are dry: I term this the “drier get hotter” mechanism. Changes in near-surface relative humidity further increase tropical land warming, with decreases in land relative humidity particularly important. The theory advances physical understanding of the tropical climate and highlights land-surface dryness as a key factor determining how extreme temperatures will respond to future climate change.

# **Amplified warming of extreme temperatures over tropical land**

Michael P. Byrne<sup>1,2</sup>

<sup>1</sup>*School of Earth & Environmental Sciences, University of St Andrews, UK*

<sup>2</sup>*Department of Physics, University of Oxford, UK*

**Extreme temperatures have warmed substantially over recent decades<sup>1,2</sup> and are projected to continue warming in response to future climate change<sup>3-5</sup>. Warming of extreme temperatures is amplified over land<sup>6-8</sup> where the impacts on human health<sup>9</sup>, wildfire risk<sup>10</sup> and food production<sup>11</sup> are most severe. Using simulations with climate models, I show that hot days over tropical land warm substantially more than the average day. For example, warming of the hottest 1% of land days is 24% larger than the time-mean warming averaged across models. The climate-change response of extreme temperatures over tropical land is interpreted using a theory based on atmospheric dynamics. According to the theory, warming is amplified for hot land days because those days are dry: I term this the “drier get hotter” mechanism. Changes in near-surface relative humidity further increase tropical land warming, with decreases in land relative humidity particularly important. The theory advances physical understanding of the tropical climate and highlights land-surface dryness as a key factor determining how extreme temperatures will respond to future climate change.**

Warming of extreme temperatures has large human<sup>9</sup> and economic impacts<sup>12</sup> particularly over land where the warming is strongest<sup>8</sup>. The land-ocean warming contrast – whereby annual-

mean near-surface temperatures increase more rapidly over land relative to ocean<sup>13–18</sup> – implies stronger warming of extreme land temperatures even in the absence of changes in temperature variability<sup>19</sup>. But increases in temperature variability with climate change further increase warming of extreme land temperatures<sup>20</sup>, with soil moisture feedbacks playing a key role in mid-latitude regions<sup>19–25</sup>. Temperature advection<sup>26–28</sup>, atmospheric circulation anomalies<sup>29</sup> and local thermodynamics<sup>30</sup> also shape extreme mid-latitude temperatures – both cold and hot – and their response to climate change.

Compared to the rapidly advancing knowledge of temperature extremes in mid-latitudes<sup>24,27–32</sup>, understanding of extreme temperatures over tropical land remains limited. Extreme temperatures in the tropics are only weakly influenced by temperature advection<sup>33</sup>, and atmospheric blocking – often the driver of extremes in mid-latitudes<sup>34</sup> – does not typically occur at low latitudes<sup>35</sup>. Soil moisture feedbacks partially account for the amplified warming of extreme temperatures relative to time-mean temperatures over tropical land<sup>23</sup>. But the effects of soil moisture on surface temperature are complex<sup>36</sup>, vary considerably across climate models<sup>19</sup> and are challenging to quantify *a priori* (i.e. without running a climate model). The limited understanding of extreme temperatures over tropical land – compounded by incomplete long-term temperature records<sup>37</sup> – compares unfavourably with the burgeoning understanding of mid-latitude temperature extremes and robust theories for precipitation and snow extremes in a changing climate<sup>38–40</sup>. With tropical regions emerging as a hotspot of intensifying temperature extremes<sup>41,42</sup>, a quantitative theory for extreme temperatures over tropical land is now needed to interpret and underpin projections from climate models and address a notable gap in understanding of the Earth system.

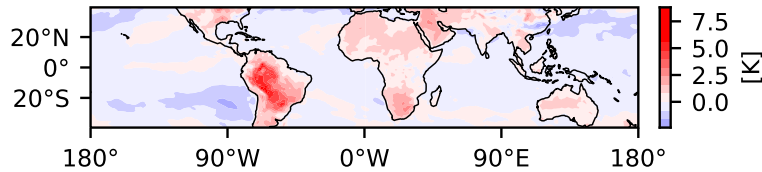


Figure 1: **Projected warming of the hottest 1% of days relative to the zonal-mean warming.**

Surface-air temperature change averaged over the hottest 1% of days at each grid cell between the *historical* (control; 1980-2000) and *ssp245* (perturbed; 2080-2100) simulations for the GFDL-CM4 model. To highlight the differing responses of extreme temperatures over land and ocean, anomalies with respect to the zonal-mean change at each latitude are shown.

### **Amplified warming of hot days**

Here I show, using simulations with climate models together with a theory based on atmospheric dynamics, that the response to climate change of extreme temperatures over tropical land – defined here as high percentiles of daily-mean near-surface temperature – is controlled by ocean warming and near-surface humidities over land and ocean. In particular, amplified warming of hot land days is driven by those days being dry; I term this the “drier get hotter” mechanism. Simulations from 18 climate models contributing to the World Climate Research Programme’s Coupled Model Intercomparison Project Phase 6<sup>43</sup> are analysed (Methods). Climate change is defined as the difference between the *historical* (or control) simulations and the Shared Socioeconomic Pathway<sup>44</sup> 4.5 (*ssp245* or perturbed) simulations. Land between 20°S and 20°N is analysed as the key assumptions underlying the theory are primarily applicable to tropical regions<sup>17,18,45</sup>.

Projected warming of extreme temperatures is amplified over tropical land (Fig. 1). Averaged across models, daily-mean near-surface tropical temperatures exceeding the 99th percentile warm by 3.6 K over land compared to 2.1 K over ocean (Fig. 2a). Warming of high percentiles of land temperature is strongly amplified relative to the mean warming<sup>46</sup> (Fig. 2b), implying a change in the shape of the temperature distribution. The higher the percentile the greater the amplification, with the hottest 1% of land days warming 24% (or 0.7K) more than the mean day. Consistent with previous work<sup>47</sup>, amplified warming of extreme temperatures is weak over tropical oceans where the hottest 1% of days warm by only 5% (or 0.1K) more than the mean day (Fig. 2).

### **A theory for the response of extreme temperatures over tropical land**

I now introduce a theory to understand the response of extreme temperatures over tropical land. In the tropics, active atmospheric convection<sup>48</sup> and weak horizontal temperature gradients above the boundary layer<sup>49</sup> constrain changes in near-surface moist static energy to be approximately equal over land and ocean<sup>18,45,50,51</sup>. Near-surface moist static energy is a function of temperature and specific humidity (Methods). Individually, temperature and specific humidity over land and ocean respond very differently to climate change in the annual mean<sup>13–18,50,52,53</sup>. But the combined response of temperature and specific humidity (specifically the moist static energy change) is approximately uniform across the tropics because of the dynamical processes connecting the atmospheres above land and ocean<sup>18</sup>.

I use this atmospheric dynamics constraint to develop a theory for the response of extreme

temperatures over tropical land to climate change (see Methods for the complete derivation). The key assumption underlying this theory is that changes in moist static energy percentiles are equal over land and ocean:

$$\delta h_L(p_h) = \delta h_O(p_h), \quad (1)$$

where  $h(p_h)$  is the  $p_h$ -th percentile of near-surface moist static energy over land (L) or ocean (O) in the control simulation and  $\delta$  denotes a change between the control and perturbed simulations. Compared to changes in percentiles of temperature or specific humidity, which show clear land-ocean contrasts, changes in moist static energy percentiles are approximately equal over land and ocean, particularly for high percentiles (Fig. 3). Ocean relative humidity is approximately constant under climate change<sup>54,55</sup> implying – together with (1) – that ocean warming constrains changes in high percentiles of moist static energy over land.

The coupling between moist static energies over land and ocean is the basis of a new theory for extreme temperatures over tropical land. To transform (1) into a theory for the land temperature response, I first assume that the change in average moist static energy of the hottest  $(100 - x)\%$  of land days ( $\delta h_L^x$ ) is equal to the change in ocean moist static energy ( $\delta h_O$ ) plus a contribution ( $\Delta h$ ) to account for hot land days becoming relatively less energetic under climate change:

$$\delta h_L^x = \delta h_O(p_h^*) + \Delta h, \quad (2)$$

where  $p_h^*$  is the moist static energy percentile over land corresponding to the average moist static energy of the hottest  $(100 - x)\%$  of land days in the control simulation [i.e.  $h_L(p_h^*) = h_L^x$ ]. [Note that  $p_h^*$  varies with temperature percentile,  $x$  (Fig. S1)]. Over ocean, hotter days are associated with larger moist static energies (Fig. S1). Small variability in ocean relative humidity implies that the change in the  $p_h^*$ -th percentile of ocean moist static energy is well approximated by changes in the  $p_h^*$ -th percentiles of ocean temperature and specific humidity (Fig. S2). But over land, where hotter days are drier<sup>56</sup> (Fig. S3), the hottest 1% of days have a moist static energy equal to approximately the median land day and become relatively less energetic as climate warms (Fig. S1). The relative decrease with warming of the moist static energy of hot land days is quantified by  $\Delta h$ , which is well approximated by changes in land relative humidity (Fig. S4b):

$$\Delta h \approx L_v (\delta r_L^x q_{L,\text{sat}}^x - \delta \overline{r_L} \overline{q_{L,\text{sat}}}), \quad (3)$$

where  $L_v$  is the latent heat of vapourisation,  $\delta r_L^x$  is the change in land pseudo relative humidity<sup>50</sup> for the hottest  $(100 - x)\%$  of days (Methods),  $q_{L,\text{sat}}^x$  is the land saturation specific humidity for the hottest  $(100 - x)\%$  of days in the control,  $\delta \overline{r_L}$  is the time- and spatial-mean change in land pseudo relative humidity and  $\overline{q_{L,\text{sat}}}$  is the mean land saturation specific humidity. Combining (2) with (3), writing changes in specific humidity in terms of changes in saturation specific humidity and relative humidity and rearranging, the land temperature change for the hottest  $(100 - x)\%$  of days is estimated as a function of physical constants, the control state and three components associated with changes in ocean temperature, ocean relative humidity and land relative humidity:

$$\delta T_L^x = \left( \frac{1}{1 + \epsilon \delta r_L^x} \right) (\gamma^{T_O} \delta T_O + \gamma^{r_O} \delta r_O - \eta \delta \bar{r}_L). \quad (4)$$

where  $\delta T_O$  is the change in the  $p_h^*$ -th percentile of ocean temperature and  $\delta r_O$  is the change in ocean relative humidity. The parameters  $\epsilon = L_v \alpha_L q_{L,\text{sat}}^x / (c_p + L_v \alpha_L q_L^x)$  and  $\eta = (\bar{q}_{L,\text{sat}} / q_{L,\text{sat}}^x) (\epsilon / \alpha_L)$  are functions of physical constants, control-state quantities and the Clausius-Clapeyron parameter  $\alpha_L$ , which quantifies the fractional sensitivity of saturation specific humidity over land to a 1K temperature change. The parameters  $\gamma^{T_O} = (c_p + L_v \alpha_O q_O) / (c_p + L_v \alpha_L q_L^x)$  and  $\gamma^{r_O} = L_v q_{O,\text{sat}} / (c_p + L_v \alpha_L q_L^x)$  are also functions of physical constants, the control state and the Clausius-Clapeyron parameter for ocean  $\alpha_O$ . The  $\gamma$  parameters represent the sensitivities of land temperature to changes in ocean temperature ( $\gamma^{T_O}$ ) and ocean relative humidity ( $\gamma^{r_O}$ ) assuming other quantities are fixed (Fig. S5).

The theory (4) captures the key features of the land temperature response across a wide range of percentiles, including the magnitude of the response (Fig. 2a) and amplified warming at high percentiles (Fig. 2b). Inter-model differences in the temperature response are also largely explained by the theory (Fig. S6). For constant land and ocean relative humidities, the theory simplifies to:

$$\delta T_{L,\delta r=0}^x = \gamma^{T_O} \delta T_O. \quad (5)$$

This fixed-relative humidity version of theory qualitatively captures the amplified warming of hot land days relative to the mean day (Fig. 2b), with the amplification driven by larger values of  $\gamma^{T_O}$

for high temperature percentiles (Fig. S5a). The sensitivity parameter  $\gamma^{To}$  is larger for hot land days because those days are drier ( $q_L^x < q_O$ ; Fig. S7) – this is the “drier get hotter” mechanism.

I have shown that amplified warming of hot days over tropical land is primarily a consequence of those days being dry in the control state. But changes in relative humidity affect the magnitude of the land temperature response across all percentiles (Fig. 2a) and the degree to which warming of hot days is amplified (Fig. 2b). Small increases in ocean relative humidity with warming (Fig. S3) – consistent with surface energy balance arguments<sup>54,55,57</sup> – marginally increase the land warming (by 0.11 K averaged across percentiles; Fig. S8). Increasing ocean relative humidity enhances land warming as it increases the moist static energy change over land compared to a fixed-relative humidity scenario.

Land relative humidity changes further increase the land temperature response (Fig. S8). Although the sensitivity of land temperature to a 1% change in land relative humidity is small compared to the sensitivity to ocean relative humidity changes (Fig. S5b), substantial decreases in land relative humidity with warming<sup>50</sup> (Fig. S3) contribute 0.38 K to the land temperature response averaged across percentiles (Fig. S8). The physical intuition for why decreases in land relative humidity strengthen warming is straightforward: For a given increase in moist static energy over land, the larger the decrease in relative humidity the larger the temperature increase is to compensate. As the for land-ocean warming contrast<sup>17</sup>, changes in land relative humidity are an important influence on the response of hot land days to climate change.

The contribution of land relative humidity changes to the land temperature response has two

components (Methods): The first quantifies the effect of a land relative humidity change on the land temperature response assuming  $\Delta h = 0$ , and the second quantifies the effect of a non-zero  $\Delta h$  [recall that  $\Delta h$  is well approximated as a function of changes in land relative humidity (3)]. Note that  $\Delta h < 0$  (Fig. S4b) meaning that hot land days become relatively less energetic under climate change. In particular, the moist static energy of the hottest 1% of land days is equal to the 52<sup>nd</sup> percentile of moist static energy in the control simulation but only the 46<sup>th</sup> percentile in the perturbed simulation (Fig. S1). The two components of the land temperature response associated with changes in land relative humidity counteract each other (Fig. S8), with the  $\Delta h$  component strongly tempering the land warming that would otherwise occur if the moist static energy percentile corresponding to hot land days stayed fixed in a changing climate (i.e. if  $\Delta h = 0$ ).

## **Discussion**

My theory based on active convection and weak horizontal temperature gradients above the boundary layer quantitatively describes the simulated response of temperature over tropical land to climate change across a wide range of percentiles. The main result from the theory is that warming is amplified for hot land days relative to the mean day: the “drier get hotter” mechanism. This mechanism provides a simple way in which to interpret changes in extreme temperatures in the tropics. The mechanism is also predictive in the sense that it emerges from the control-state contrast in specific humidity between hot and less-hot days and is not reliant on running a climate model. Amplified warming at high percentiles suggests that trends in the temperature of hot land

days may be an early indicator of climate change in the tropics.

The magnitude of tropical land warming is strongly enhanced by changes in relative humidity, with decreases in land relative humidity particularly important. Extending the theory to incorporate the influence of land relative humidity changes as a function of the ocean warming and control state<sup>18,50</sup> would be a natural next step, as would be the application of the theory to individual regions and to other climate perturbations (e.g. the El Niño/Southern Oscillation).

## Methods

**Simulations.** The following 18 models are analysed: ACCESS-CM2, ACCESS-ESM1-5, BCC-CSM2-MR, CanESM5, CESM2-WACCM, CNRM-CM6-1, CNRM-ESM2-1, GFDL-CM4, GFDL-ESM4, HadGEM3-GC31-LL, INM-CM4-8, INM-CM5-0, KACE-1-0-G, MIROC-ES2L, MPI-ESM1-2-LR, MRI-ESM2-0, NorESM2-LM and UKESM1-0-LL. Daily-mean near-surface temperature and specific humidity from the *historical* (control; 1980–2000) and *ssp245* (perturbed; 2080–2100) simulations are used to investigate the response of tropical temperatures to climate change and evaluate the theory. The *ssp245* simulations broadly assume that emissions of greenhouse gases will continue at historical trends<sup>44</sup> resulting in a radiative forcing of  $4.5 \text{ W/m}^2$  by 2100.

Percentiles are computed at each latitude individually by aggregating daily-mean quantities over time and longitude. Before plotting, percentiles are averaged from 20°S to 20°N with area weighting. Percentiles over land and ocean are calculated separately. Land is defined as grid

cells where the percentage area occupied by land is greater than 50%; otherwise the grid cell is defined as ocean. Twenty six percentiles of temperature, specific humidity and moist static energy between the 0th and the 99th percentiles are computed; spline interpolation is used to estimate the percentiles between these computed values. The theory, derived below, is applied at each latitude individually before averaging the results from 20°S to 20°N. Saturation specific humidity is calculated based on Bolton (1980)<sup>58</sup>.

**Derivation of theory for extreme temperatures over tropical land.** The key assumption underpinning the theory for the response of extreme temperatures over tropical land to climate change is that percentiles  $p_h$  of moist static energy  $h$  change equally over land (L) and ocean (O):  $\delta h_L(p_h) = \delta h_O(p_h)$ . My focus is on hot days over land; the change in average moist static energy (in J/kg) of the hottest  $(100 - x)\%$  of land days between the control and perturbed simulations is given by:

$$\delta h_L^x = c_p \delta T_L^x + L_v \delta q_L^x, \quad (6)$$

where  $c_p = 1004.6$  J/kg/K is the specific heat capacity of air at constant pressure,  $L_v = 2.5 \times 10^6$  J/kg is the latent heat of vapourisation,  $T_L^x$  is the near-surface land temperature (in kelvin) averaged over the hottest  $(100 - x)\%$  of days and  $q_L^x$  is the average near-surface land specific humidity (in kg/kg) conditioned on  $T_L^x$ .

Defining  $p_h^*$  to be the moist static energy percentile over land corresponding to the average moist static energy of the hottest  $(100 - x)\%$  of days in the control simulation [i.e.  $h_L(p_h^*) = h_L^x$ ]

and using the assumption of equal changes in moist static energy percentiles over land and ocean, the change in moist static energy of the hottest  $(100 - x)\%$  days is expressed as:

$$\delta h_L^x = \delta h_O(p_h^*) + \Delta h, \quad (7)$$

where  $\Delta h = h_L^{\text{pert}}(p_h^* + \delta p_h^*) - h_L^{\text{pert}}(p_h^*)$  quantifies the effect of a change in the percentile of land moist static energy to which hot land days correspond ( $\delta p_h^*$ ) on the moist static energy of these hot days. Note that  $h_L^{\text{pert}}$  is the moist static energy in the perturbed simulation. As climate warms, hot land days become relatively less energetic ( $\delta p_h^* < 0$ ; Figs. S1 and S4a) implying that  $\Delta h < 0$  (Fig. S4b). The relative decrease in the moist static energy of hot land days with warming (compared to a scenario where  $\Delta h = 0$ ) reduces the absolute increases in moist static energy on those days, and has an important tempering influence on the response of extreme temperatures over tropical land.

Through (7), changes in the moist static energy of hot land days are related to changes in ocean moist static energy. Specifically, it is the change in the  $p_h^*$ -th percentile of ocean moist static energy that is relevant for hot land days. Over oceans, higher temperatures are associated with higher moist static energies (Fig. S1) implying that the change in the  $p_h^*$ -th percentile of ocean moist static energy can be written to good approximation as a function of changes in the  $p_h^*$ -th percentiles of temperature and specific humidity (Fig. S2):

$$\delta h_O(p_h^*) \approx c_p \delta T_O(p_h^*) + L_v \delta q_O(p_h^*). \quad (8)$$

Combining (6) and (8), equation (7) can be written as:

$$c_p \delta T_L^x + L_v \delta q_L^x = c_p \delta T_O(p_h^*) + L_v \delta q_O(p_h^*) + \Delta h. \quad (9)$$

Defining pseudo relative humidities<sup>50</sup> over land [ $r_L^x = q_L^x/q_{L,\text{sat}}^x$ ] and ocean [ $r_O = q_O(p_h^*)/q_{O,\text{sat}}(p_h^*)$ ], where  $q_{L,\text{sat}}^x$  and  $q_{O,\text{sat}}(p_h^*)$  are the saturation specific humidities calculated using  $T_L^x$  and  $T_O(p_h^*)$ , respectively, changes in specific humidity over land and ocean are written in terms of temperature and relative humidity:

$$\delta q_L^x = q_{L,\text{sat}}^x \delta r_L^x + \alpha_L q_{L,\text{sat}}^x \delta T_L^x + \alpha_L q_{L,\text{sat}}^x \delta r_L^x \delta T_L^x \quad (10)$$

$$\delta q_O \approx q_{O,\text{sat}} \delta r_O + \alpha_O q_O \delta T_O, \quad (11)$$

where  $\alpha_L = (\delta q_{L,\text{sat}}^x/q_{L,\text{sat}}^x)/\delta T_L^x$  and  $\alpha_O = (\delta q_{O,\text{sat}}/q_{O,\text{sat}})/\delta T_O$  are the fractional sensitivities of land and ocean saturation specific humidities, respectively, to a 1K temperature change. For the change in ocean specific humidity (11), the nonlinear term associated with temperature and relative humidity changes has been omitted as it is negligible, but this term is substantial over land and is retained (10). Inserting expressions (10) and (11) into (9), dividing both sides by  $c_p + L_v \alpha_L q_{L,\text{sat}}^x$  and rearranging, I obtain the following expression for the land temperature response:

$$\delta T_L^x = \left( \frac{1}{1 + \epsilon \delta r_L^x} \right) (\gamma^{T_O} \delta T_O + \gamma^{r_O} \delta r_O - [\epsilon/\alpha_L] \delta r_L^x + \Delta h), \quad (12)$$

where  $\epsilon = L_v \alpha_L q_{L,\text{sat}}^x / (c_p + L_v \alpha_L q_{L,\text{sat}}^x)$ . The parameters

$$\gamma^{To} = \frac{c_p + L_v \alpha_O q_O}{c_p + L_v \alpha_L q_L^x} \text{ and} \quad (13)$$

$$\gamma^{ro} = \frac{L_v q_{O,\text{sat}}}{c_p + L_v \alpha_L q_L^x} \quad (14)$$

quantify the sensitivities of land temperature to changes in ocean temperature and ocean relative humidity, respectively, for fixed land relative humidity and  $\Delta h = 0$  (Fig. S5).

The  $\Delta h$  term in (12) is estimated as a function of the control land temperature and changes in land relative humidity. First, I approximate  $\Delta h = h_L^{\text{pert}}(p_h^* + \delta p_h^*) - h_L^{\text{pert}}(p_h^*)$  as a Taylor series about  $p_h = p_h^*$ :

$$\Delta h = [h_L(p_h^* + \delta p_h^*) - h_L(p_h^*)] + [\delta h_L(p_h^* + \delta p_h^*) - \delta h_L(p_h^*)] \quad (15)$$

$$\approx \delta p_h^* \left( \left. \frac{\partial h_L}{\partial p_h} \right|_{p_h=p_h^*} + \frac{\partial}{\partial p_h} \delta h_L \Big|_{p_h=p_h^*} \right). \quad (16)$$

To estimate  $\delta p_h^*$ , I linearise the land moist static energy distribution in the control simulation about the mean value:

$$h_L(p_h) \approx \beta_1(p_h - \overline{p_h}) + \overline{h_L}, \quad (17)$$

where  $\overline{h_L}$  is the time- and spatial-mean moist static energy over land in the control simulation,  $\overline{p_h}$  is the moist static energy percentile corresponding to that mean value and  $\beta_1 = \partial h_L / \partial p_h|_{p_h=\overline{p_h}}$  is the slope of the tangent to the control moist static energy distribution over land at  $p_h = \overline{p_h}$  (Fig. S9). The average moist static energy of the hottest  $(100 - x)\%$  of land days is given by:

$$h_L^x = c_p T_L^x + L_v q_L^x. \quad (18)$$

Combining (17) and (18), dropping the approximation symbol associated with (17) and noting that  $h_L(p_h^*) = h_L^x$  by definition, I find:

$$\beta_1(p_h^* - \bar{p}_h) + \bar{h}_L = c_p T_L^x + L_v q_L^x. \quad (19)$$

Writing  $T_L^x = \bar{T}_L + T_L'$ ,  $r_L^x = \bar{r}_L + r_L'$  and  $q_{L,\text{sat}}^x = \bar{q}_{L,\text{sat}} + q'_{L,\text{sat}}$  [where  $\bar{(\ )}$  denotes the time- and spatial-mean and  $(\ )'$  denotes a departure from that mean], substituting into (19) and rearranging, I derive an expression for  $p_h^*$ :

$$p_h^* = \frac{1}{\beta_1} [c_p T_L' + L_v(\bar{r}_L q'_{L,\text{sat}} + r_L' \bar{q}_{L,\text{sat}} + r_L' q'_{L,\text{sat}})] + \bar{p}_h. \quad (20)$$

Changes in the moist static energy percentile corresponding to the hottest  $(100 - x)\%$  of land days (i.e.  $\delta p_h^*$ ) are well approximated by truncating a linearised form of (20) to two terms (Fig. S4a):

$$\delta p_h^* \approx \frac{L_v}{\beta_1} (\delta r_L^x q_{L,\text{sat}}^x - \delta \bar{r}_L \bar{q}_{L,\text{sat}}). \quad (21)$$

Inserting this estimate for  $\delta p_h^*$  into (16), defining  $\beta_2 = \partial h_L / \partial p_h|_{p_h=p_h^*}$  to be the slope of the tangent to  $h_L(p_h)$  at  $p_h = p_h^*$ , neglecting changes in  $\beta_2$  with warming (i.e. assuming  $\delta \beta_2 \ll \beta_2$ ) and further assuming  $\beta_1 \approx \beta_2$  (Fig. S9),  $\Delta h$  is well approximated by (Fig. S4b):

$$\Delta h \approx L_v (\delta r_L^x q_{L,\text{sat}}^x - \overline{\delta r_L} \overline{q_{L,\text{sat}}}). \quad (22)$$

Substituting (22) into (12) and rearranging, I derive an expression for the temperature response of the hottest  $(100 - x)\%$  of land days as a function of physical constants, control-state quantities and four components associated with  $\Delta h$  and changes in ocean temperature, ocean relative humidity and land relative humidity:

$$\begin{aligned} \delta T_L^x = & \left( \frac{1}{1 + \epsilon \delta r_L^x} \right) \left( \underbrace{\gamma^{T_O} \delta T_O}_{\delta T_O \text{ comp.}} + \underbrace{\gamma^{r_O} \delta r_O}_{\delta r_O \text{ comp.}} + \underbrace{[\epsilon/\alpha_L][\delta r_L^x - \overline{\delta r_L} \overline{q_{L,\text{sat}}}/q_{L,\text{sat}}^x]}_{\Delta h \text{ comp.}} \right) \\ & - \underbrace{\left( \frac{1}{1 + \epsilon \delta r_L^x} \right) [\epsilon/\alpha_L] \delta r_L^x}_{\delta r_L \text{ comp.}}. \end{aligned} \quad (23)$$

The four components of the land temperature response are shown in Figure S8 along with their sum, which is approximately equal to the full expression for  $\delta T_L^x$  (23). The  $\Delta h$  and  $\delta r_L$  components are both functions of changes in land relative humidity and can be combined into a total land relative humidity component:

$$\delta r_L^{\text{total}} \text{ comp.} = \delta r_L \text{ comp.} + \Delta h \text{ comp.} = - \left( \frac{1}{1 + \epsilon \delta r_L^x} \right) \eta \overline{\delta r_L}, \quad (24)$$

where  $\eta = (\epsilon/\alpha_L)(\overline{q_{L,\text{sat}}}/q_{L,\text{sat}}^x)$ . Using (24), I arrive at the final form of the theory [see (4) in the main text]. Finally, based on (24) and taking  $\delta r_L^x = \overline{r_L}$  for simplicity, I define the sensitivity parameter

$$\gamma^{rL} = -\frac{\eta}{1 + \epsilon} \quad (25)$$

which quantifies the sensitivity of land temperature to changes in mean land relative humidity (Fig. S5b).

1. Perkins, S. E., Alexander, L. V. & Nairn, J. R. Increasing frequency, intensity and duration of observed global heatwaves and warm spells. *Geophys. Res. Lett.* **39** (2012).
2. Donat, M. G. *et al.* Updated analyses of temperature and precipitation extreme indices since the beginning of the twentieth century: The HadEX2 dataset. *J. Geophys. Res.: Atmos.* **118**, 2098–2118 (2013).
3. Fischer, E. M., Beyerle, U. & Knutti, R. Robust spatially aggregated projections of climate extremes. *Nature Climate Change* **3**, 1033–1038 (2013).
4. Sillmann, J., Kharin, V. V., Zhang, X., Zwiers, F. W. & Bronaugh, D. Climate extremes indices in the CMIP5 multimodel ensemble: Part 1. Model evaluation in the present climate. *J. Geophys. Res.: Atmos.* **118**, 1716–1733 (2013).
5. Fischer, E. M. & Knutti, R. Anthropogenic contribution to global occurrence of heavy-precipitation and high-temperature extremes. *Nature Climate Change* **5**, 560–564 (2015).
6. Orłowsky, B. & Seneviratne, S. I. Global changes in extreme events: regional and seasonal dimension. *Climatic Change* **110**, 669–696 (2012).

7. Seneviratne, S. I. *et al.* Changes in climate extremes and their impacts on the natural physical environment. *Managing the Risks of Extreme Events and Disasters to Advance Climate Change Adaptation. A Special Report of Working Groups I and II of the Intergovernmental Panel on Climate Change (IPCC)* 109–230 (2012).
8. Seneviratne, S. I., Donat, M. G., Pitman, A. J., Knutti, R. & Wilby, R. L. Allowable CO<sub>2</sub> emissions based on regional and impact-related climate targets. *Nature* **529**, 477–483 (2016).
9. Patz, J. A., Campbell-Lendrum, D., Holloway, T. & Foley, J. A. Impact of regional climate change on human health. *Nature* **438**, 310–317 (2005).
10. Liu, Y., Stanturf, J. & Goodrick, S. Trends in global wildfire potential in a changing climate. *Forest Ecology and Management* **259**, 685–697 (2010).
11. Schlenker, W. & Roberts, M. J. Nonlinear temperature effects indicate severe damages to US crop yields under climate change. *Proc. Natl. Acad. Sci.* **106**, 15594–15598 (2009).
12. Burke, M., Hsiang, S. M. & Miguel, E. Global non-linear effect of temperature on economic production. *Nature* **527**, 235–239 (2015).
13. Sutton, R. T., Dong, B. & Gregory, J. M. Land/sea warming ratio in response to climate change: IPCC AR4 model results and comparison with observations. *Geophys. Res. Lett.* **34** (2007). L02701.
14. Lambert, F. H. & Chiang, J. C. H. Control of land-ocean temperature contrast by ocean heat uptake. *Geophys. Res. Lett.* **34** (2007). L13704.

15. Joshi, M. M., Gregory, J. M., Webb, M. J., Sexton, D. M. H. & Johns, T. C. Mechanisms for the land/sea warming contrast exhibited by simulations of climate change. *Climate Dyn.* **30**, 455–465 (2008).
16. Byrne, M. P. & O’Gorman, P. A. Land-ocean warming contrast over a wide range of climates: Convective quasi-equilibrium theory and idealized simulations. *J. Climate* **26**, 4000–4016 (2013).
17. Byrne, M. P. & O’Gorman, P. A. Link between land-ocean warming contrast and surface relative humidities in simulations with coupled climate models. *Geophys. Res. Lett.* **40**, 5223–5227 (2013).
18. Byrne, M. P. & O’Gorman, P. A. Trends in continental temperature and humidity directly linked to ocean warming. *Proc. Natl. Acad. Sci.* **115**, 4863–4868 (2018).
19. Vogel, M. M. *et al.* Regional amplification of projected changes in extreme temperatures strongly controlled by soil moisture-temperature feedbacks. *Geophys. Res. Lett.* **44**, 1511–1519 (2017).
20. Schär, C. *et al.* The role of increasing temperature variability in European summer heatwaves. *Nature* **427**, 332–336 (2004).
21. Diffenbaugh, N. S. & Ashfaq, M. Intensification of hot extremes in the United States. *Geophys. Res. Lett.* **37** (2010).
22. Mueller, B. & Seneviratne, S. I. Hot days induced by precipitation deficits at the global scale. *Proc. Natl. Acad. Sci.* **109**, 12398–12403 (2012).

23. Seneviratne, S. I. *et al.* Impact of soil moisture-climate feedbacks on CMIP5 projections: First results from the GLACE-CMIP5 experiment. *Geophys. Res. Lett.* **40**, 5212–5217 (2013).
24. Miralles, D. G., Teuling, A. J., Van Heerwaarden, C. C. & De Arellano, J. V.-G. Mega-heatwave temperatures due to combined soil desiccation and atmospheric heat accumulation. *Nat. Geosci.* **7**, 345–349 (2014).
25. Lorenz, R. *et al.* Influence of land-atmosphere feedbacks on temperature and precipitation extremes in the GLACE-CMIP5 ensemble. *J. Geophys. Res.: Atmos.* **121**, 607–623 (2016).
26. Screen, J. A. Arctic amplification decreases temperature variance in northern mid-to high-latitudes. *Nature Climate Change* **4**, 577–582 (2014).
27. Schneider, T., Bischoff, T. & Płotka, H. Physics of changes in synoptic midlatitude temperature variability. *J. Climate* **28**, 2312–2331 (2015).
28. Tamarin-Brodsky, T., Hodges, K., Hoskins, B. J. & Shepherd, T. G. Changes in Northern Hemisphere temperature variability shaped by regional warming patterns. *Nat. Geosci.* **13**, 414–421 (2020).
29. Wehrli, K., Guillod, B. P., Hauser, M., Leclair, M. & Seneviratne, S. I. Identifying key driving processes of major recent heat waves. *J. Geophys. Res.: Atmos.* **124**, 11746–11765 (2019).
30. Vargas Zeppetello, L. R. & Battisti, D. S. Projected increases in monthly midlatitude summertime temperature variance over land are driven by local thermodynamics. *Geophys. Res. Lett.* **47** (2020).

31. McKinnon, K. A., Rhines, A., Tingley, M. P. & Huybers, P. The changing shape of Northern Hemisphere summer temperature distributions. *J. Geophys. Res.: Atmos.* **121**, 8849–8868 (2016).
32. Linz, M., Chen, G. & Hu, Z. Large-scale atmospheric control on non-Gaussian tails of mid-latitude temperature distributions. *Geophys. Res. Lett.* **45**, 9141–9149 (2018).
33. Holmes, C. R., Woollings, T., Hawkins, E. & De Vries, H. Robust future changes in temperature variability under greenhouse gas forcing and the relationship with thermal advection. *J. Climate* **29**, 2221–2236 (2016).
34. Pfahl, S. & Wernli, H. Quantifying the relevance of atmospheric blocking for co-located temperature extremes in the Northern Hemisphere on (sub-) daily time scales. *Geophys. Res. Lett.* **39** (2012).
35. Liu, Q. On the definition and persistence of blocking. *Tellus A* **46**, 286–298 (1994).
36. Seneviratne, S. I. *et al.* Investigating soil moisture-climate interactions in a changing climate: A review. *Earth-Sci. Rev.* **99**, 125–161 (2010).
37. Donat, M. G. & Alexander, L. V. The shifting probability distribution of global daytime and night-time temperatures. *Geophys. Res. Lett.* **39**, L14707 (2012).
38. O’Gorman, P. A. & Schneider, T. The physical basis for increases in precipitation extremes in simulations of 21st-century climate change. *Proc. Natl. Acad. Sci.* **106**, 14773–14777 (2009).

39. O’Gorman, P. A. Contrasting responses of mean and extreme snowfall to climate change. *Nature* **512**, 416–418 (2014).
40. Pfahl, S., O’Gorman, P. A. & Fischer, E. M. Understanding the regional pattern of projected future changes in extreme precipitation. *Nature Climate Change* **7**, 423–427 (2017).
41. Perkins-Kirkpatrick, S. E. & Gibson, P. B. Changes in regional heatwave characteristics as a function of increasing global temperature. *Scientific Reports* **7**, 12256 (2017).
42. Harrington, L. J. & Otto, F. E. L. Reconciling theory with the reality of African heatwaves. *Nature Climate Change* **10**, 796–798 (2020).
43. Eyring, V. *et al.* Overview of the Coupled Model Intercomparison Project Phase 6 (CMIP6) experimental design and organization. *Geosci. Model Dev.* **9**, 1937–1958 (2016).
44. O’Neill, B. C. *et al.* The Scenario Model Intercomparison Project (ScenarioMIP) for CMIP6. *Geosci. Model Dev.* **9**, 3461–3482 (2016).
45. Zhang, Y. & Fueglistaler, S. How tropical convection couples high moist static energy over land and ocean. *Geophys. Res. Lett.* **47**, e2019GL086387 (2020).
46. Duan, S. Q., Findell, K. L. & Wright, J. S. Three regimes of temperature distribution change over dry land, moist land and oceanic surfaces. *Geophys. Res. Lett.* e2020GL090997 (2020).
47. Johnson, N. C. & Xie, S.-P. Changes in the sea surface temperature threshold for tropical convection. *Nature Geosci.* **3**, 842–845 (2010).

48. Emanuel, K. A., Neelin, D. J. & Bretherton, C. S. On large-scale circulations in convecting atmospheres. *Quart. J. Roy. Meteor. Soc.* **120**, 1111–1143 (1994).
49. Sobel, A. H. & Bretherton, C. S. Modeling tropical precipitation in a single column. *J. Climate* **13**, 4378–4392 (2000).
50. Byrne, M. P. & O’Gorman, P. A. Understanding decreases in land relative humidity with global warming: conceptual model and GCM simulations. *J. Climate* **29**, 9045–9061 (2016).
51. Berg, A. M. *et al.* Land-atmosphere feedbacks amplify aridity increase over land under global warming. *Nat. Climate Change* **6**, 869–874 (2016).
52. Sherwood, S. C. & Fu, Q. A drier future? *Science* **343**, 737–739 (2014).
53. Chadwick, R., Good, P. & Willett, K. M. A simple moisture advection model of specific humidity change over land in response to SST warming. *J. Climate* **29**, 7613–7632 (2016).
54. Held, I. M. & Soden, B. J. Water vapor feedback and global warming. *Annu. Rev. Energy Environ.* **25**, 441–475 (2000).
55. Schneider, T., O’Gorman, P. A. & Levine, X. J. Water vapor and the dynamics of climate changes. *Rev. Geophys.* **48**, RG3001 (2010).
56. Fischer, E. M. & Knutti, R. Robust projections of combined humidity and temperature extremes. *Nat. Climate Change* **3**, 126–130 (2013).
57. Boer, G. J. Climate change and the regulation of the surface moisture and energy budgets. *Climate Dyn.* **8**, 225–239 (1993).

58. Bolton, D. The computation of equivalent potential temperature. *Mon. Wea. Rev.* **108**, 1046–1053 (1980).

**Acknowledgements** This project has received funding from the European Union’s Horizon 2020 research and innovation programme under the Marie Skłodowska-Curie Grant Agreement 794063 and the UK Natural Environment Research Council’s Grant NE/T006269/1. The author thanks Emily Newsom, Laure Zanna and Yi Zhang for helpful discussions. All analyses were performed using Pangeo, a community platform for Big Data geoscience (<https://pangeo.io>).

**Competing Interests** The author declares that he has no competing financial interests.

**Correspondence** Correspondence and requests for materials should be addressed to the author (email: [mpb20@st-andrews.ac.uk](mailto:mpb20@st-andrews.ac.uk)).

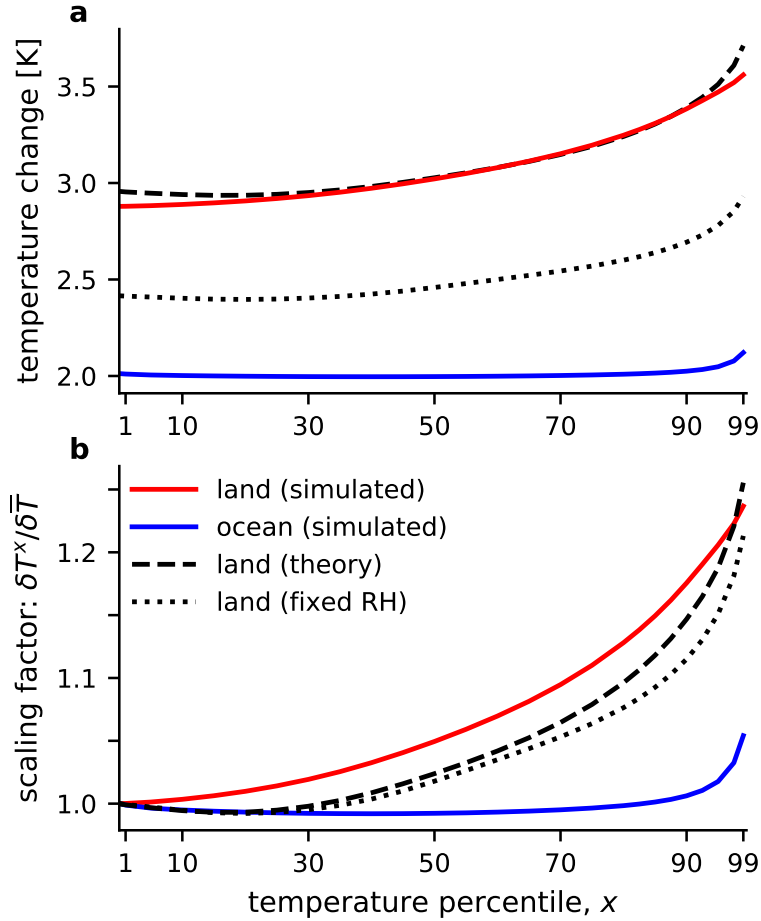


Figure 2: **Climate model projections and theoretical estimates of tropical land temperature responses across percentiles.** Multimodel-mean (a) near-surface temperature change and (b) scaling factor between the control and perturbed simulations for a range of daily-mean temperature percentiles ( $x$ ) over land (red) and ocean (blue). Temperatures are averaged over the hottest  $(100 - x)\%$  of land or ocean days. The scaling factor is defined as the temperature change at each percentile ( $\delta T^x$ ) normalised by the time- and spatial-mean temperature change ( $\overline{\delta T}$ ). Theory estimates of the land temperature change and scaling factor are also shown [dashed lines, see (4)] along with a version of the theory assuming fixed relative humidities over land and ocean [dotted lines, see (5)]. In this and subsequent figures, quantities are spatially averaged from  $20^\circ\text{S}$  to  $20^\circ\text{N}$ .

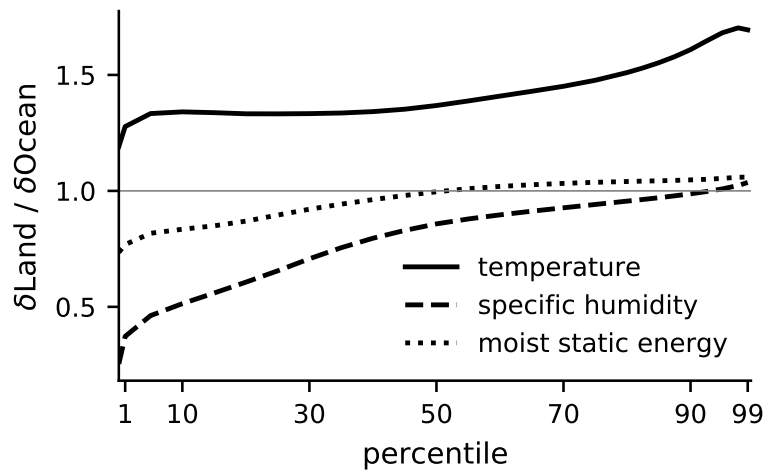


Figure 3: **Ratios of land-to-ocean changes in tropical temperature, specific humidity and moist static energy.** Land-to-ocean ratios of multimodel-mean changes in percentiles of near-surface temperature (solid black), specific humidity (dashed black) and moist static energy (dotted black) between the control and perturbed simulations.

# Amplified warming of extreme temperatures over tropical land

## Supplementary information

Michael P. Byrne

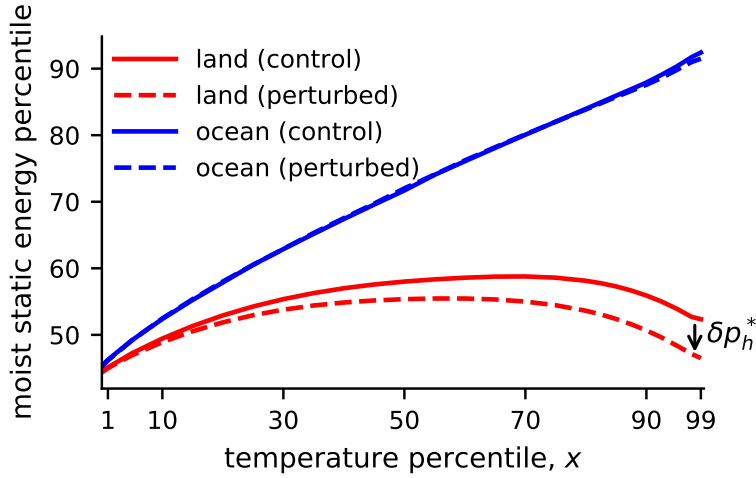


Figure S1: Moist static energy percentiles ( $y$ -axis) corresponding to the average moist static energy of days exceeding the given temperature percentile on the  $x$ -axis over land (red) and ocean (blue). Solid and dashed lines denote the control and perturbed simulations, respectively. The decrease with warming of the moist static energy percentile to which hot land days corresponds is indicated ( $\delta p_h^*$ ).

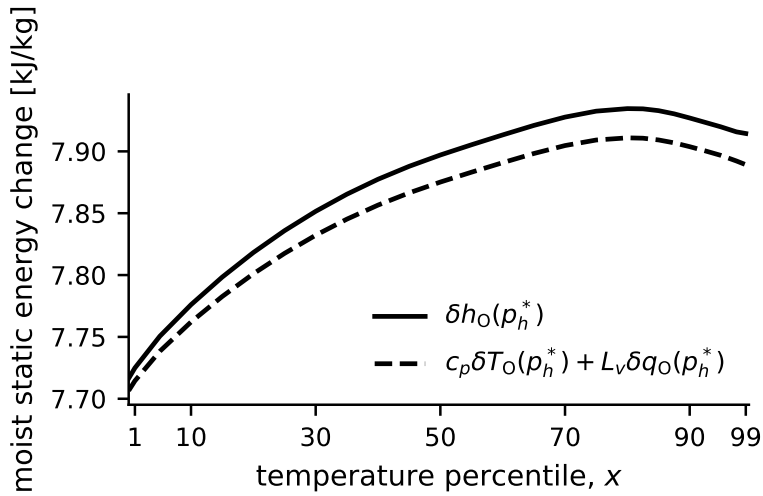


Figure S2: Change in the  $p_h^*$ -th percentile of ocean moist static energy (solid) and an estimate of this change using the  $p_h^*$ -th percentiles of ocean temperature and specific humidity (dashed). The fractional differences between the solid and dashed lines are less than 0.5% for all percentiles.

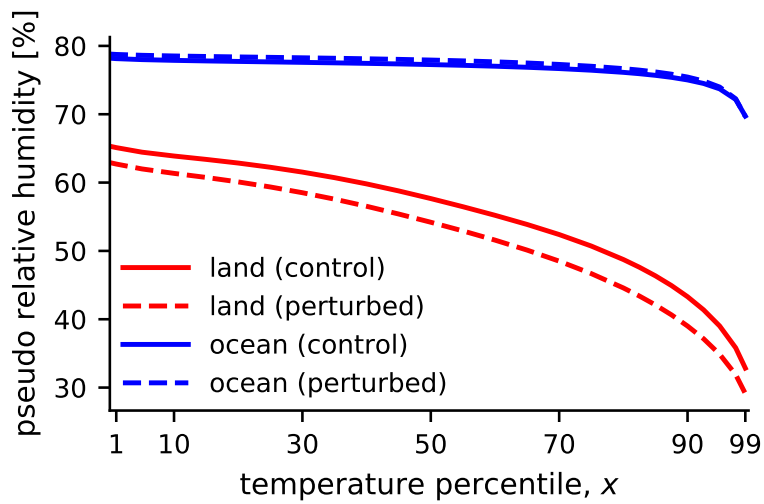


Figure S3: Pseudo relative humidity over land (red) and ocean (blue) for the control (solid) and perturbed simulations (dashed). Over land, pseudo relative humidity is defined as the average specific humidity for the hottest  $(100 - x)\%$  of days divided by the corresponding average saturation specific humidity (Methods). Over ocean, pseudo relative humidity is defined as the  $p_h^*$ -th percentile of specific humidity divided by the  $p_h^*$ -th percentile of saturation specific humidity. Note that  $p_h^*$  is the percentile of land moist static energy in the control simulation equal to the average moist static energy of the hottest  $(100 - x)\%$  of land days.

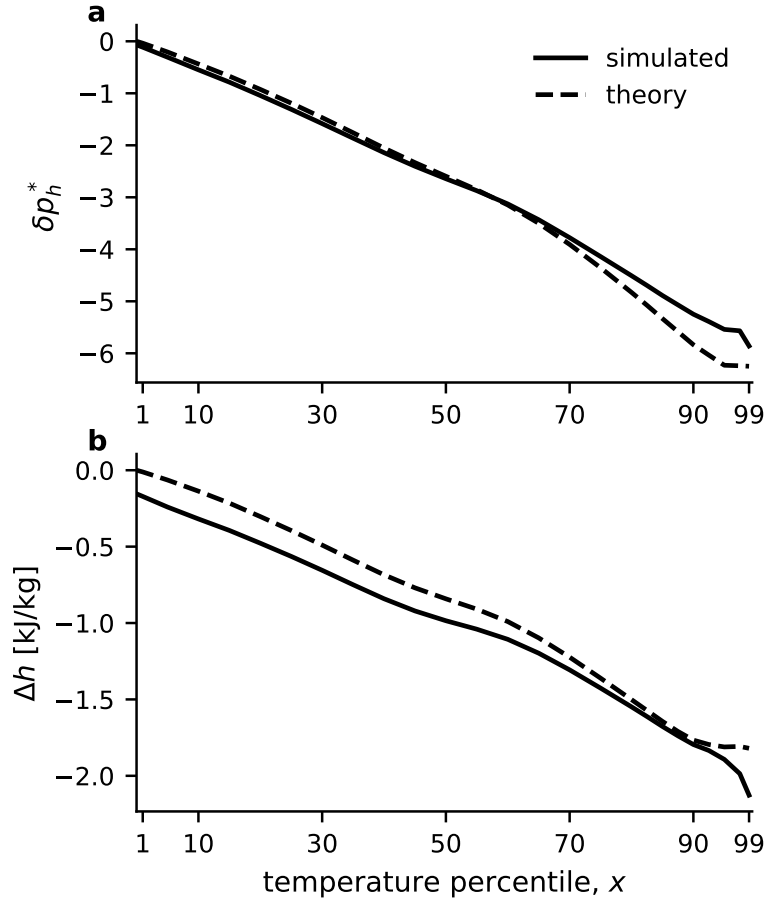


Figure S4: Simulated (solid) and theory estimates (dashed) of (a) changes in the percentile of land moist static energy equal to the average moist static energy of the hottest  $(100 - x)\%$  of land days (i.e.  $\delta p_h^*$ ) and (b)  $\Delta h = h_L^{pert}(p_h^* + \delta p_h^*) - h_L^{pert}(p_h^*)$ . The theory estimates in panels (a) and (b) are computed using equations (21) and (3), respectively.

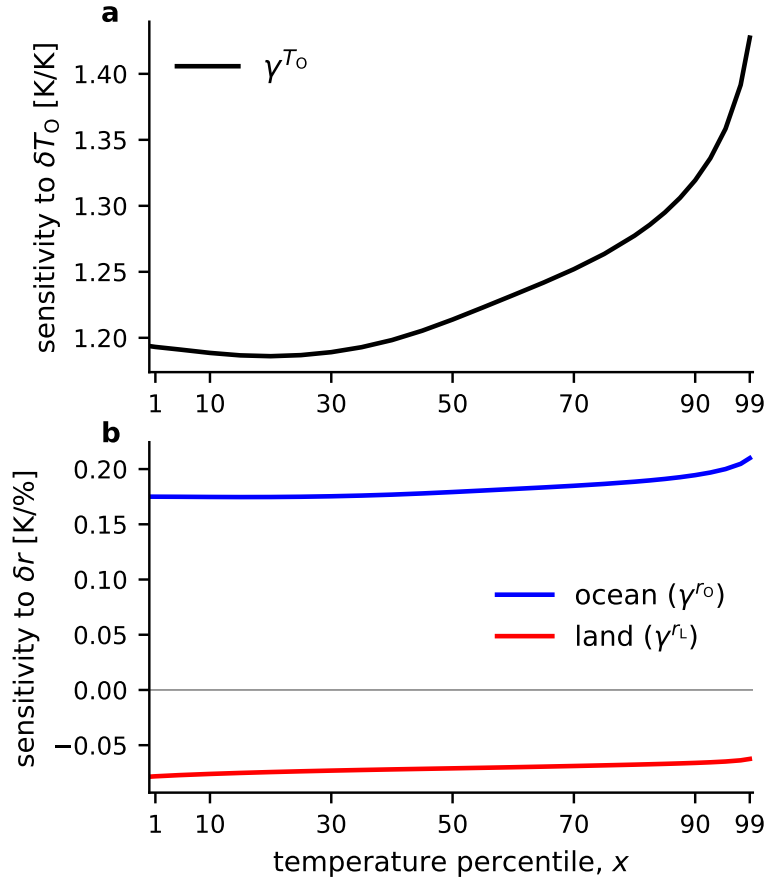


Figure S5: Parameters quantifying the sensitivities of land temperature to changes in (a) ocean temperature and (b) ocean (blue) and land relative humidities (red). The sensitivity parameters  $\gamma^{T_o}$ ,  $\gamma^{r_o}$  and  $\gamma^{r_L}$  are defined by equations (13), (14) and (25), respectively.

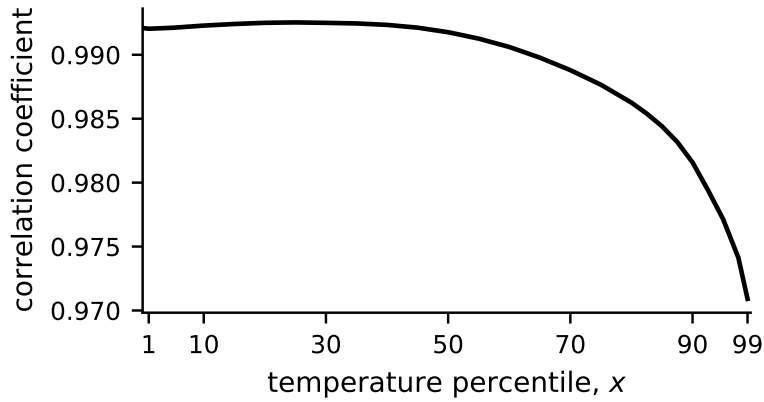


Figure S6: Correlation coefficients between simulated and estimated changes [using (4)] in average temperature for the hottest  $(100 - x)\%$  of land days across climate models.

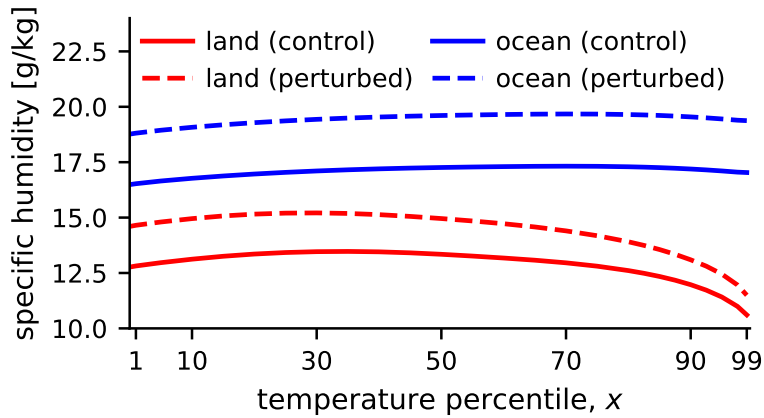


Figure S7: Specific humidity over land (red) and ocean (blue) for the control (solid) and perturbed simulations (dashed). Over land, the average specific humidities for the hottest  $(100 - x)\%$  of days are shown. Over ocean, the  $p_h^*$ -th percentile of specific humidity in each simulation is plotted.

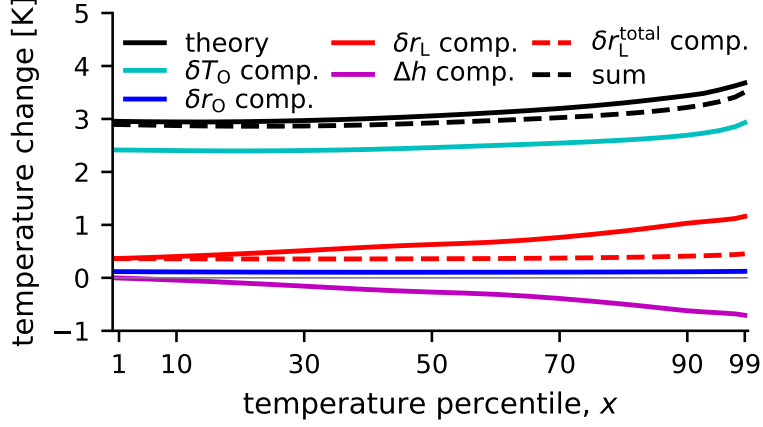


Figure S8: Theory estimate of the land temperature change [solid black, see (4)] and the four contributions to the theory (23) due to changes in ocean temperature (cyan), ocean relative humidity (blue), land relative humidity (solid red) and  $\Delta h$  (magenta). The sum of the four contributions (dashed black) is approximately equal to the full theory. The combined effect of changes in land relative humidity and  $\Delta h$  [see (24)] is indicated by the dashed red line.

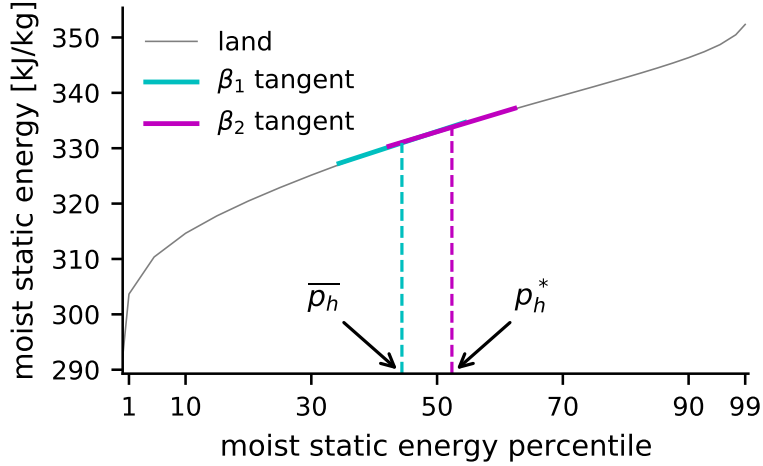


Figure S9: Land moist static energy in the control simulation vs moist static energy percentile (gray). The parameters  $\beta_1$  (cyan) and  $\beta_2$  (magenta) are the slopes of the tangents to  $h_L(p_h)$  at  $\bar{p}_h$  and  $p_h^*$ , respectively.